Carbon 178 (2021) 649–656

Contents lists available at ScienceDirect

Carbon

journal homepage: www.elsevier.com/locate/carbon

Research Article

Flash graphene from rubber waste

Paul A. Advincula [a], Duy Xuan Luong [a], Weiyin Chen [a], Shivaranjan Raghuraman [b], Rouzbeh Shahsavari [b, **], James M. Tour [a, c, d, *]

[a] Department of Chemistry, Rice University, 6100 Main Street MS 222, Houston, TX, 77005, USA
[b] C-Crete Technologies, 13000 Murphy Road, Unit 102, Stafford, TX, United States
[c] Smalley-Curl Institute, NanoCarbon Center and the Welch Institute for Advanced Materials, Rice University, United States
[d] Department of Materials Science and NanoEngineering, Rice University, 6100 Main Street, Houston, TX, 77005, USA

ARTICLE INFO

Article history:
Received 22 January 2021
Received in revised form
1 March 2021
Accepted 1 March 2021
Available online 28 March 2021

Keywords:
Flash graphene
Rubber waste
Turbostratic graphene
Upcycling
Flash joule heating

ABSTRACT

Most conventional production processes for graphene are time-consuming, solvent-intensive, and energetically demanding. To circumvent these limitations for mass production, flash Joule heating (FJH) has been shown to be an effective method to synthesize graphene. Here, methods for optimizing production of graphene from rubber waste feedstocks are shown. Through careful control of system parameters, such as pulse voltage and pulse time, turbostratic flash graphene (tFG) can be produced from rubber waste. It is characterized by Raman spectroscopy, X-ray diffraction and thermogravimetric analysis. The resulting tFG can be easily exfoliated and dispersed into various solvents because of its turbostratic arrangement. Addition of tFG into Portland cement results in a significant increase in the compressive strength of the composite. From a materials perspective, FJH offers a facile and inexpensive method for producing high quality tFG from rubber waste materials, which would otherwise be disposed of in landfills or burned for fuel. FJH allows for upcycling of low-value rubber waste into high-value carbon nanomaterials for use as reinforcing additives.

1. Introduction

The disposal of processed rubber results in an abundance of waste. According to the U.S. Tire Manufacturers Association, 43% of scrap tires in the U.S. are used as fuel, 25% are used for ground rubber applications, and 16% are stored in landfills. The remaining materials are used for various civil engineering applications [1]. These applications include rubber-reinforced asphalt [2] or Portland cement composites [3]. Every year, over 800 million waste tires are produced worldwide. The majority of these tires are placed into landfills or burned for fuel. The lack of high-value recycling products for rubber waste shows that new methods are needed for use of these waste materials.

Each year, over 30 billion tons of concrete are produced, outpacing per capita production of any other material. By mass, concrete is the most consumed material in the world, aside from water [4]. While developing countries invest in new infrastructure, developed countries face the need to replace or upgrade existing infrastructure, further increasing the demand for concrete. Concrete production has far-reaching environmental impacts. Cement production accounts for 2–3% of total global energy use and 9% of global annual industrial water withdrawals [5]. The production of 1 ton of cement results in an equivalent amount of carbon dioxide emissions. As a result, cement production is responsible for 8–9% of anthropogenic carbon dioxide emissions. For these reasons, improvement of the performance of cementitious materials in order to reduce consumption of these components is highly desirable. A variety of reinforcing additives, such glass fibers, carbon nanotubes, and graphene have been applied in concrete composites to control crack initiation/propagation and improve mechanical properties. Addition of graphene and graphene oxide derivatives has greatly enhanced the strength of cement paste [6].

Conventional methods of graphene production are time-, energy-, or chemical-intensive, resulting in a high cost of production and processing. Current synthetic techniques include mechanical or chemical exfoliation [7], chemical vapor deposition, chemical oxidation or reduction [8,9], shear exfoliation [10] and other techniques [11].

* Corresponding author. Department of Chemistry, Rice University, 6100 Main Street MS 222, Houston, TX, 77005, USA.
** Corresponding author.
E-mail addresses: rouzbeh@ccretetech.com (R. Shahsavari), tour@rice.edu (J.M. Tour).

https://doi.org/10.1016/j.carbon.2021.03.020
0008-6223/

We recently developed a method for graphene synthesis through flash Joule heating (FJH), which uses an electric current to form high-quality turbostratic flash graphene (tFG) [12]. This process is compatible with waste rubber feedstocks and is less expensive than conventional synthetic techniques. Here, we optimize the conversion of waste rubber to tFG. Pyrolyzed rubber tire-derived carbon black (TCB) is obtained by heating rubber tires at low temperatures in an atmosphere devoid of oxygen. No actual burning occurs under these conditions, allowing the tire to be broken down into TCB, steel, and hydrocarbon oil and gas. We convert TCB or a blend of carbon black (CB) with shredded rubber tires (CB:SRT) into graphene and show that tFG can be used as a reinforcement additive in cementitious materials because of its solubility in various solvents.

2. Methods

Given that high voltage is used during the FJH process, it is imperative that long rubber gloves be worn at all times. Additionally, physical contact is only made when the sample box is isolated from the bank of capacitors. See additional safety precautions in our prior work [12,13].

2.1. Materials

Milled TCB (DEN1-S190604-2B) was provided by Ergon Asphalt and Emulsion Inc. and used as received. CB (BP-2000) was purchased from Cabot Corporation and used as received. SRT was prepared by using an angle grinder to reduce a Michelin rubber (DOT-B3WC-02NX-3317) tire into < 2 mm size particles. CB and SRT were then blended in a mortar and pestle in order to obtain a homogeneous blend of 5% CB with 95% SRT, resulting in the CB:SRT feedstock. By itself, SRT is not conductive enough to be subjected to FJH. Adding 5% CB to the feedstock reduces the resistance of the SRT from the MΩ range to <100 Ω. This enables the CB:SRT feedstock to be effectively FJH. xGnP graphite nanoplatelets (xGnP-15, serial #: 5051209) were obtained from XG Sciences and were used as received. Commercial graphene was obtained from Tianyuan Empire Materials & Technologies, Shatin, Hong Kong and was used as received.

2.2. Raman spectroscopy

All Raman spectra were collected using tFG samples that were ground with a mortar and pestle to ensure homogeneity, with no exposure to solvent. A Renishaw Raman microscope and a 532-nm laser with a power of 5 mW was used with a 50× objective lens to collect local Raman spectra and mapping. Samples were scanned from 100 to 3200 cm^{-1}.

2.3. XRD

All XRD patterns were collected using tFG samples that were ground with a mortar and pestle to ensure homogeneity, with no exposure to solvent. A Rigaku D/Max Ultima II Powder XRD 6s and Rigaku D/Max Ultima II Powder XRD 1s were used to collect XRD patterns. Zero background sample holders were used, along with a scan width of 0.02°/step and a scan rate of 1°/min from 5 to 90°.

2.4. TGA

All TGA thermograms were collected using tFG samples that were ground with a mortar and pestle to ensure homogeneity, with no exposure to solvent. Alumina pans were used in a Mettler Toledo TGA/DSC 3+ system. Data was collected over the temperature range of 50–900 °C. From 50 to 425 °C, the heating rate was kept at 15 °C/min. From 425 to 725 °C, the heating rate was decreased to 5 °C/min, since this is the area of interest. From 725 to 900 °C, the heating rate was again returned to 15 °C/min. All samples were run under an atmosphere of air.

2.5. Preparation of tFG dispersions in solvents

tFG, commercial graphene, graphite, graphite nanoplatelets, and exfoliated graphite materials were dispersed in a variety of solvents including mineral oil, vegetable oil, WD-40, Synfluid polyalphaolefin (PAO) 6 cSt, PAO 9 cSt, and 1% Pluronic F-127 in water at a concentration of 5 g L^{-1}. The dispersions were sonicated in an ultrasonic bath for 1 h to obtain well-dispersed solutions. The samples were allowed to settle for 1 week before being centrifuged for 30 min at 5000 rpm to remove aggregated materials. PAO 6 cSt (DCS-052419) and PAO 9 cSt (DCS-113018) were procured from Chevron Phillips and used as received. WD-40, Wesson Vegetable Oil, and McKesson Mineral Oil (Heavy Liquid Petrolatum) were all used as received.

2.6. Preparation of tFG:Cement composites

TCB tFG and CB:SRT tFG was dispersed in solutions of 1% Pluronic F-127 in water at various concentrations. This solution was then agitated for 15 min at 5000 rpm using a shear mixer (Silverson L5MA). The suspension of tFG in water was then blended with Portland cement at a water:cement ratio of 0.4. This slurry was used to cast 2.45 cm^3 cement pastes and 10.16 × 20.32 cm concrete cylinders to undergo compressive strength measurements. After 24 h the samples were placed in water to cure for 24 h. The compressive strength of the samples was then measured in 7 and 28 days. For each ratio, three samples were prepared and tested.

2.7. Compressive strength testing

Compression strength tests were conducted using a Forney Variable Frequency Drive automatic machine with dual load cells for maximum accuracy.

2.8. Estimated energy cost for FJH conversion into tFG

The following equation is used to calculate the energy required for the FJH process:

$$E = (V_i^2\text{-}V_f^2) \text{ x } C / 2 \text{ x } M$$

For this example, values taken from the conversion of TCB into tFG are used. Here, E is the energy required for conversion. V_i and V_f are the initial and final voltages of the FJH process (150 and 50 V, respectively). C is the capacitance available to the FJH system (0.06 F). M is the mass of each batch used for conversion into tFG (0.5 g).

$$E = (150^2\text{-}50^2) \text{ x } 0.06 / 2 \times 0.5 = 1.2 \text{ kJ/g} = 302 \text{ kWh/ton}$$

Assuming that the cost of electricity is ~$0.02/kWh for industrial rates in Texas, the cost in electricity to convert 1 ton of TCB into tFG is ~$6.05, which is far cheaper than conventional methods of producing bulk graphene. Hence, the estimate of <$100 in electrical costs is generous.

3. Results and discussion

The rubber source is placed between two graphite plug

electrodes that were further contacted by copper electrodes, as shown in Fig. 1. An electrical pulse is then discharged through the sample, causing the material to reach ~3000 K in <0.5 s. This causes carbon-carbon bonds to break and rearrange into high-quality graphene. Rapid cooling of the system leads to formation of the kinetically stable tFG rather than graphene with AB-stacked morphology. When using TCB or CB:SRT as a carbon source, ~70% or ~47% of the material is recovered as tFG, respectively. Non-carbon materials sublime out during this process, as evidenced by the loss of non-carbon elements in XPS of the samples (Fig. S1). The conversion process would require < $100 of electrical energy per ton of starting carbon (See Methods for calculation) [12].

Several parameters such as the pulse voltage and pulse time can be adjusted when using the FJH system. Varying the pulse voltage and time will alter the peak current and total energy in the sample, which will in turn affect the peak temperature and time spent at that peak temperature, respectively.

Raman spectroscopy is a valuable tool for analyzing the quality of graphene. When analyzing graphene, three prominent Raman spectroscopy active phonon modes are usually observed: 2D (~2700 cm^{-1}), G (~1580 cm^{-1}), and D (~1350 cm^{-1}). The 2D mode results from an overtone of the in-plane transverse optic branch (iTO). The G band is a response to an in-plane phonon mode that usually appears in graphitic carbon. The D peak appears when there are structural defects or graphene edges present in the sample. By examining the intensity ratio of the 2D peak to the G peak, one can deduce the quality and number of layers of AB-stacked graphene. In single-layer graphene, the 2D peak displays a single Lorentzian profile. As the number of layers increases, the 2D peak splits into separate modes that combine, resulting in a wider, shorter, and higher frequency 2D peak when compared to single-layer graphene. Generally, a higher I_{2D}/I_G ratio indicates graphene with fewer layers, since the 2D intensity will increase as the number of graphene layers decreases. Graphene with fewer layers is desirable, since more layers usually results in loss of desirable 2D material properties, due to increased interlayer electron transport. However, tFG being turbostratic, has an increased interlayer spacing between sheets and the graphene sheets are rotated with respect to one another. Because of this, the 2D intensity for tFG actually increases as the number of graphene layers increases. Despite this, tFG with an increased number of layers still retains its desirable 2D material properties because interlayer electron transport is inhibited by the increased interlayer spacing. The I_D/I_G ratio can also be used to analyze the degree of disorder present in the sample, wherein a higher ratio indicates a greater amount of disorder (Fig. 2).

Varying the voltage of the FJH pulse can significantly affect the conversion of the carbon feedstock to tFG, as seen in Fig. 2a,c. Changing the voltage of the flash pulse changes the temperature of the sample. The resulting temperature spike can be estimated by fitting the black-body radiation spectrum between 600 and 100 nm [12]. By varying the pulse voltage from 170 to 130 V, different degrees of graphene quality and conversion can be achieved, since the peak current changes.

As the voltage increases, the peak current, and in turn the peak temperature reached in the sample, increases as well. The best quality tFG is produced at a voltage of ~140 V–150 V, as indicated by the high I_{2D}/I_G ratios for CB:SRT and TCB, respectively. At voltages >150 V, this ratio tends to decrease. This is likely because AB-stacking is thermodynamically more stable so the material continues to rearrange, which may account for the observed decrease in the I_{2D}/I_G ratio [14]. Beyond certain voltages, the quartz tube cannot withstand the peak current-induced temperature, resulting in cracking of the quartz tube and sample loss. However, decreasing voltage usually results in lower conversion, with more of the original feedstock remaining after the initial pulse, as shown by the increased D peak and reduced I_{2D}/I_G ratio, indicating the presence

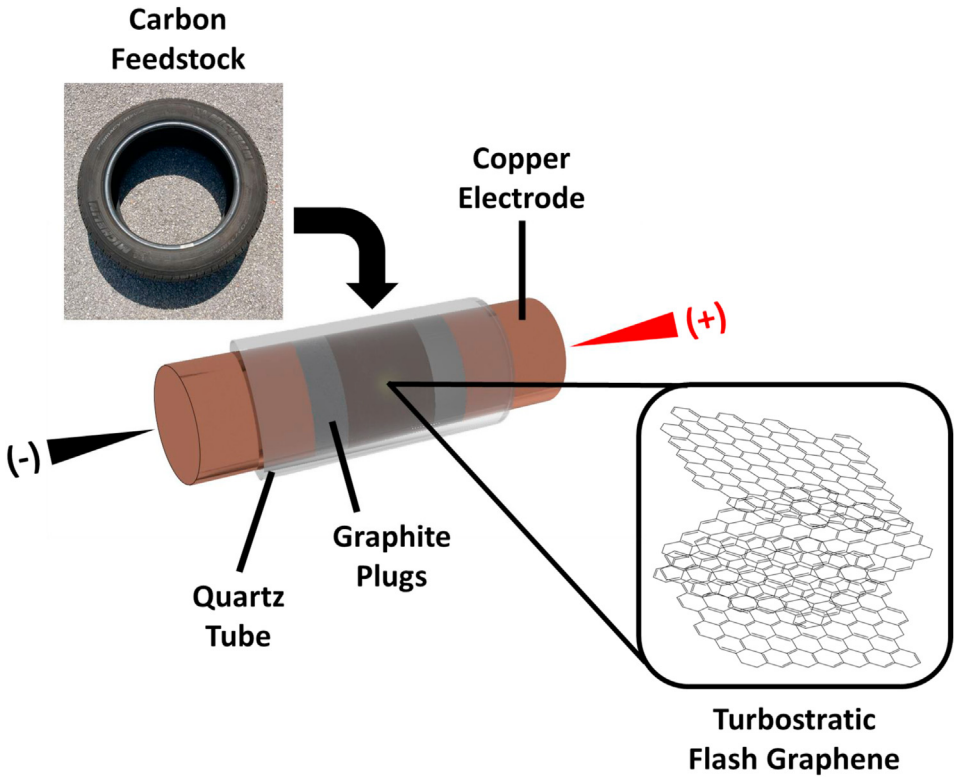

Fig. 1. Schematic depicting the sample setup of the FJH system for conversion of rubber waste into tFG. (A colour version of this figure can be viewed online.)

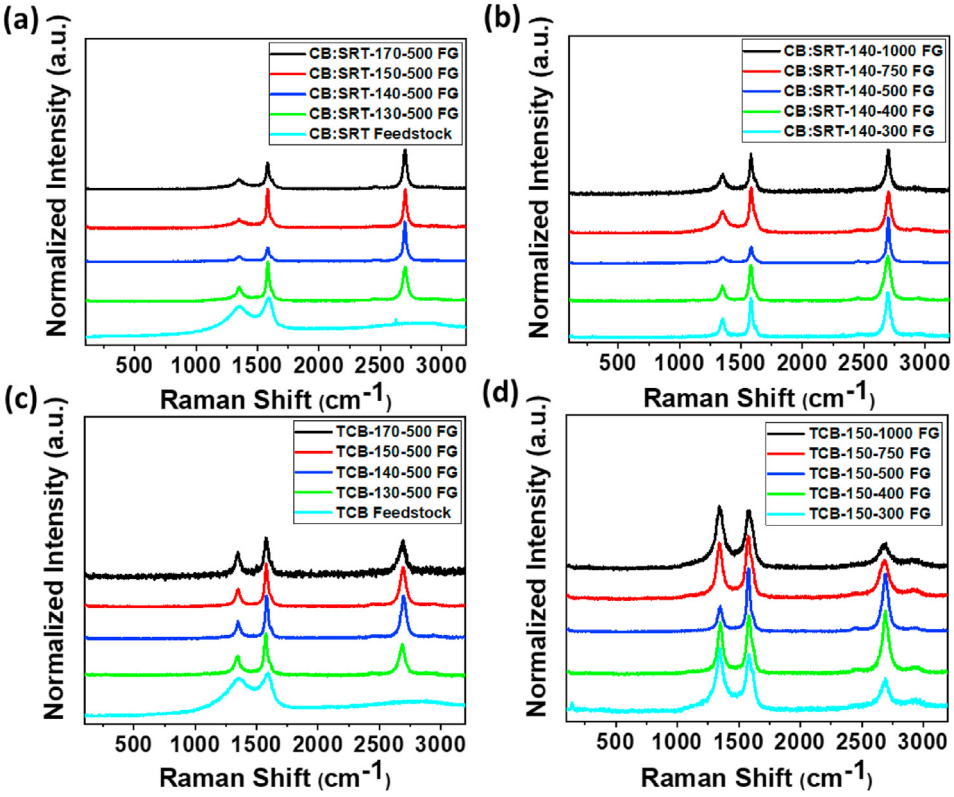

Fig. 2. Raman spectral analysis based upon FJH parameter changes. The label format "Sample-X-Y FG" is used, where "Sample" is the carbon feedstock, X is the pulse voltage in V, Y is the pulse time in ms, and FG is tFG. Raman spectra of CB:SRT tFG with varying (a) pulse voltages and (b) pulse times. Raman spectra of TCB tFG with varying (c) pulse voltages and (d) pulse times. A 532-nm laser with 50× magnification is used to acquire Raman spectra. (A colour version of this figure can be viewed online.)

of amorphous carbon. This is most likely because the temperature achieved is insufficient to convert material throughout the tube. Hence, optimization of the pulse voltage used during the FJH process is paramount to achieving sufficient conversion without excessive AB-stacking.

Pulse time was modulated between 300 and 1000 ms, as shown in Fig. 2b,d. Changing pulse time has a minimal effect on the peak current but is more useful for tuning the total amount of energy directed through the sample, which also affects the temperature [12]. Increasing pulse times allow for more energy to go through the sample while maintaining the same peak current for the initial transformation. As seen in Fig. 2b,d, a pulse time of ~500 ms produces tFG with the highest I_{2D}/I_G ratio. Samples with a pulse time >500 ms have a less intense 2D peak, indicating that, given time, graphene flakes will favor AB-stacking, which is more thermodynamically stable. However, insufficient pulse time results in a lower degree of conversion of the starting material, as indicated by the large D peak that appears in samples flashed with pulse times <500 ms (Figs. S2 and S3). This likely occurs because the pulse time is insufficient to allow the entire material to heat to the requisite temperature for conversion.

After optimization, FJH of TCB results in ~70% process yield with >95% purity. This TCB tFG has an average I_{2D}/I_G ratio of 0.752. FJH of CB:SRT results in ~47% process yield with >95% purity. CB:SRT tFG has an average I_{2D}/I_G ratio of 0.83. Process yield is calculated as the percentage of feedstock remaining after the FJH pulse, purity is calculated as the percentage of Raman spectra taken from the sample that displayed a I_{2D}/I_G ratio with a value > 0.5. As the pulse voltage is increased, the average I_{2D}/I_G ratio, as well as purity of the samples increases and then decreases. A similar trend is also observed when varying the pulse time. (Fig. S4). This trend is seen for both the TCB and CB:SRT feedstocks.

Thermogravimetric analysis (TGA) (Fig. 3) can be used to estimate the conversion of feedstock material into FG. The CB:SRT and TCB feedstocks experienced major degradation starting at 250 °C and 400 °C, respectively, with only 5% and 20% material remaining after thermal degradation, respectively. In contrast, samples of tFG remained stable until ~500 °C, indicating that FG is more thermally stable than the parent feedstock. Additionally, the lack of degradation in the FG samples at 250 °C and 400 °C for CB:SRT tFG and TCB tFG, respectively, indicates that the CB:SRT and TCB feedstocks were converted from amorphous carbon into tFG. Compared to reduced graphene oxide prepared using the Hummer's method, tFG products are more oxidatively stable [15].

Most bulk graphene derived from graphite is AB-stacked, as shown in Fig. 4a. AB-stacked graphene has an interlayer spacing of 3.35 Å since electron-rich areas of graphene overlap electron-deficient areas. As the number of AB-stacked layers increases, the desirable 2D properties of graphene are lost. The tFG produced by FJH is turbostratic, meaning that the individual graphene layers have rotated about the axis normal to the graphene sheets. This results in an interlayer spacing of 3.45 Å for tFG since overlapping electron-rich areas drive the layers apart, as seen in Fig. 4b [16]. The increase in interlayer spacing makes tFG much easier to exfoliate and disperse into single sheets compared to AB-stacked graphene. This spacing enables tFG to retain the desirable 2D properties of monolayer graphene even with an increased number of layers, due to the decreased electron mobility between layers.

Raman spectroscopy is helpful in determining the turbostratic nature of tFG by examining the combination Raman modes that appear between 1700 and 2200 cm^{-1} as seen in Fig. 4c and d [17,18]. Particularly, the combinations of in-plane transverse acoustic (iTA)/

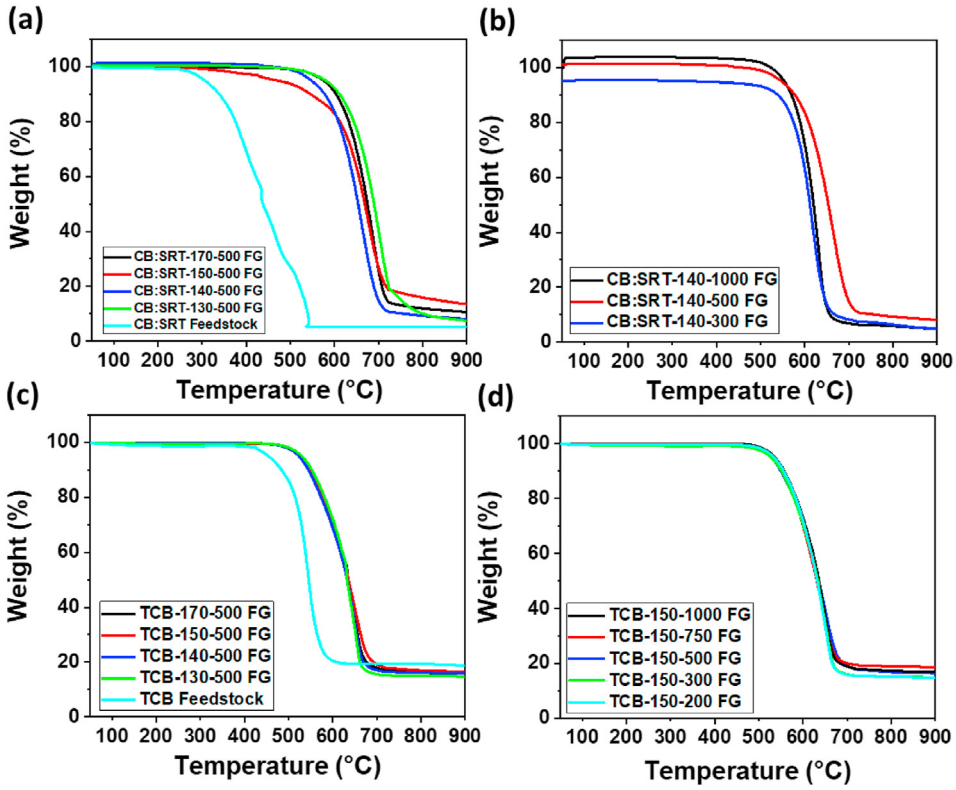

Fig. 3. TGA thermograms for CB:SRT tFG with varying (a) pulse voltage and (b) pulse time. CB:SRT was blended with a 5:95 ratio of CB to SRT. TGA thermograms for TCB tFG with varying (c) pulse voltage and (d) pulse time. These measurements were acquired in an atmosphere of air. From 50 to 425 °C, the heating rate was kept at 15 °C/min. From 425 to 725 °C, the heating rate was decreased to 5 °C/min, since this is the area of interest. From 725 to 900 °C, the heating rate was again returned to 15 °C/min. (A colour version of this figure can be viewed online.)

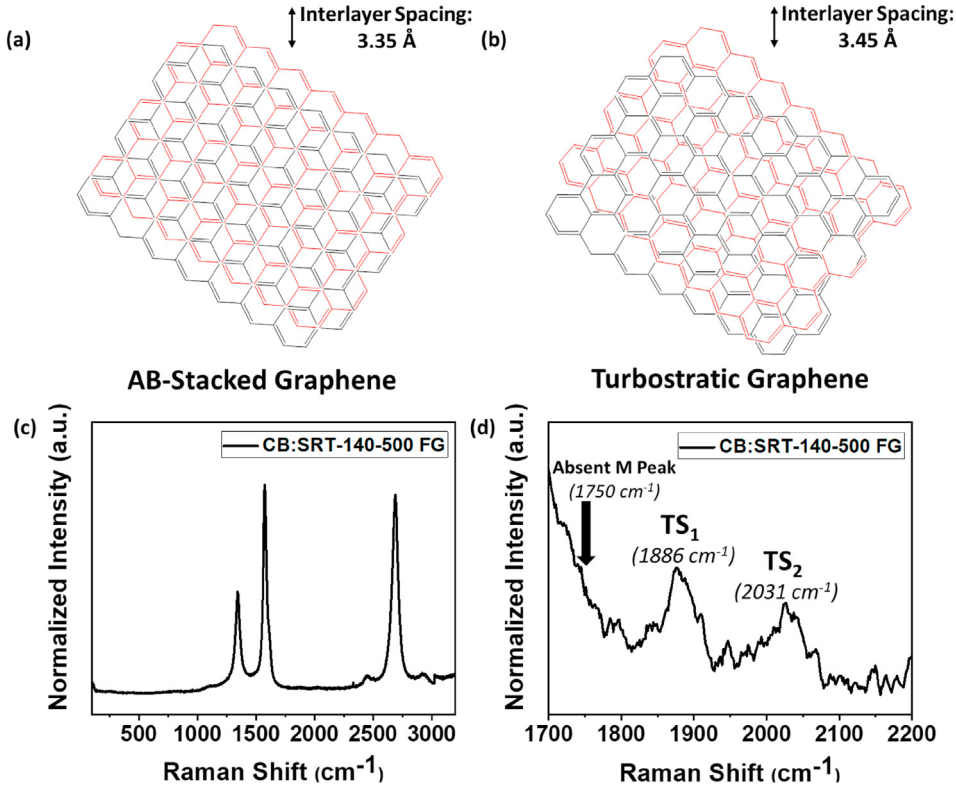

Fig. 4. Depiction of (a) AB-stacked graphene and (b) turbostratic graphene. (c) Representative Raman spectrum for CB:SRT tFG with (d) focus on the region between 1700 cm^{-1} and 2200 cm^{-1} to display the TS_1 and TS_2 peaks in this region. (A colour version of this figure can be viewed online.)

longitudinal optic (LO) (iTALO$^-$, iTALO$^+$), in-plane transverse optic (iTO)/longitudinal acoustic (LA) (iTOLA), and LO + LA modes that appear in turbostratic FG become much more difficult to resolve for AB-stacked graphene. Here, the iTALO$^-$ mode is designated as the TS_1 band (1886 cm^{-1}) and the iTOLA/LOLA modes are designated as the TS_2 band (2031 cm^{-1}). These bands shift to a higher frequency than in single-layer graphene due to stiffening of phonon modes. The presence of these bands is considered to be a signature of tFG [12]. Additionally, in AB-stacked graphene, the M band is detected as an overtone of the oTO mode, an infrared-active out-of-plane mode [17]. The absence of this band in the Raman spectrum indicates a lack of AB-stacking [19]. The presence of the TS_1 and TS_2 bands at 1886 and 2031 cm^{-1}, respectively, as well as the absence of a M band at 1750 cm^{-1} are all signatures of the turbostratic nature of tFG [12].

X-ray diffraction (XRD) also allows for analysis of the stacking of tFG sheets. tFG can randomly shift and rotate about the normal axis of graphene layers. This motion changes the interlayer spacing and shape of the atomic layers. As crystallite size decreases or graphene sheets curve, the diffraction angle of the (002) peak that appears at ~26° decreases, while the FWHM of the (002) peak increases [20]. Additionally, rotation of graphene layers causes the three-dimensional lines, with the exception of (00l) lines, to disappear. These remaining lines instead shift to lower diffraction angles as a result of local positive fluctuation of the interlayer spacing. We see this effect with our sample in Fig. 5a. The FWHM of the (002) peak for TCB tFG and CB:SRT tFG increases, relative to graphite and graphite nanoplatelets, indicating smaller crystallite size and/or curvature of graphene layers, as shown in Fig. 5a. The three-dimensional lines, such as (101) and (102) that appear at 45° and 50°, respectively, decrease in size, which can be more easily seen in Fig. 5b. The XRD patterns for each sample of tFG appear in Fig. S5.

Commercial graphene, exfoliated graphite and tFG were each separately dispersed in 1% Pluronic F-127 in water before being bath sonicated and centrifuged. Pluronic F-127 was selected since it is used as a dispersing agent for additives in cementitious materials. After one week, the tFG dispersions remained stable and well-dispersed, while commercial graphene and exfoliated graphite precipitated out of solution within 24 h, as shown in Fig. 5c.

The solubility of each tFG sample in different solvents was tested by dispersing TCB-150-500 tFG and CB:SRT-140-500 tFG in mineral oil, vegetable oil, WD-40, 1% Pluronic F-127 in water, PAO 6, and PAO 9 at a concentration of 5 mg/mL. The samples were then bath sonicated and centrifuged. Even after 1 week, these solutions remain stable and well-dispersed, as shown in Fig. 5d for TCB-150-500 tFG. This is likely due to the small size of the tFG flakes (~33 nm), as seen in Fig. S6. Additionally, the average interlayer spacing of the TCB and CB:SRT tFG flakes are shown to be ~3.45 Å, further supporting the conclusion that the TCB and CB:SRT are converted into turbostratic material. The interlayer distance calculations for each material are shown in Figs. S7 and S8. Because of the wide range of solvents in which tFG can be dispersed, tFG can easily be integrated into plastic and cement production processes that use these solvents.

To test the efficacy of tFG as a reinforcing additive, composites of tFG and cement were prepared using varying concentrations of TCB-150-500 tFG and CB:SRT-140-500 tFG. These composites were then tested after 7 and 28 days of curing. After 7 days, 34% and 30% increases in compressive strength were achieved using 0.1 wt% TCB tFG and 0.05 wt% CB:SRT tFG, respectively, as shown in Fig. 6a. After 28 days, addition of 0.1 wt% TCB tFG and CB:SRT tFG increased the compressive strength of the cement by 31% and 30%, respectively, as shown in Fig. 6b. Even a low wt% loading of tFG in cement can greatly increase the compressive strength of the matrix material. Flash Joule heating can economically convert negative-value feedstocks into graphene for use as a reinforcing additive. The ~30% increase in concrete strength leads to use of less concrete for construction, hence mitigating manufacturing energy and CO_2 emissions associated with the production of concrete.

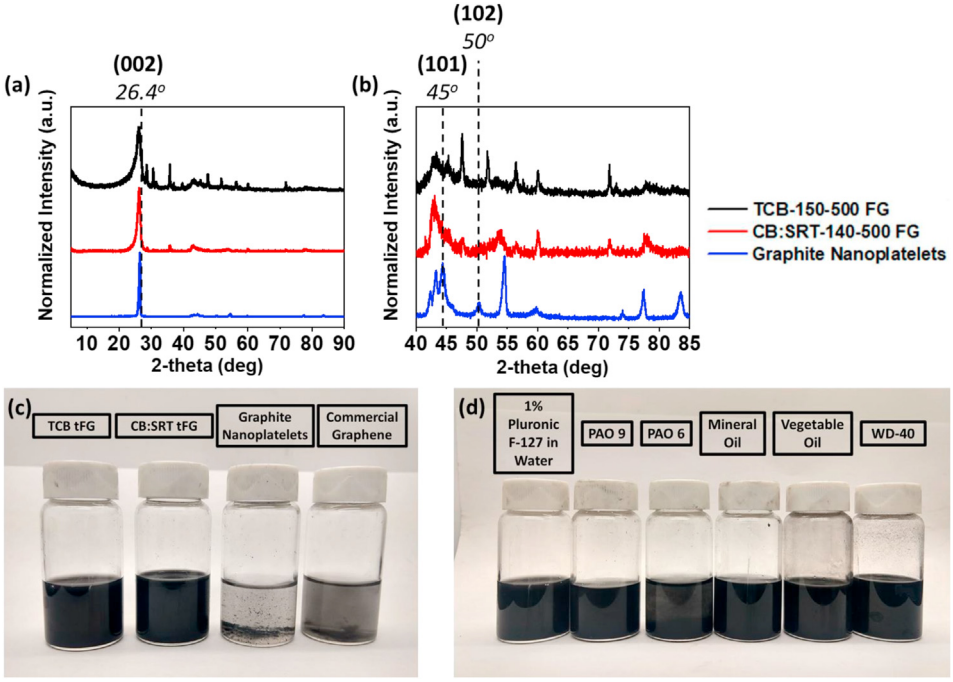

Fig. 5. (a) XRD patterns of different samples with (b) expansion of the region between 40 and 85°. (c) 5 mg/mL dispersions of TCB tFG, CB:SRT tFG, graphite nanoplatelets, and commercial graphene in a solution of 1% Pluronic F-127 in water. (d) 5 mg/mL dispersions of TCB-150-500 tFG in various solvents. These samples were left in dispersion for 1 week. (A colour version of this figure can be viewed online.)

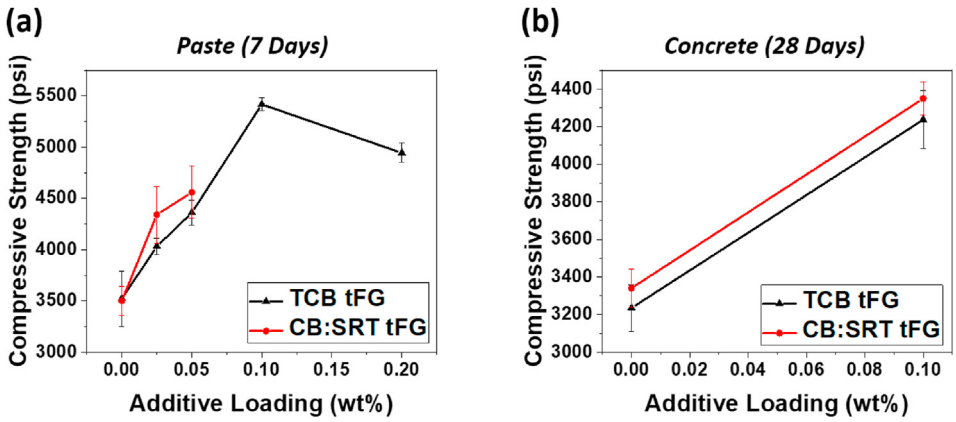

Fig. 6. Compressive strength of TCB and CB:SRT tFG of (a) a cement paste in 7 days and (b) concrete in 28 days. (A colour version of this figure can be viewed online.)

4. Conclusions

Rubber waste in the form of TCB and CB:SRT has been successfully converted into tFG through optimization of the FJH process. Varying the pulse voltage and pulse time of the FJH process resulted in tFG with high I_{2D}/I_G ratios. Raman spectroscopy and XRD indicates that the resulting FG is turbostratic. tFG has been found to disperse much more easily than AB-stacked carbon materials in water with 1% Pluronic F-127. tFG also remained effectively dispersed for a long period of time in a variety of solvents. This suggests that tFG can likely be better dispersed in cement or plastic composites, possibly resulting in stronger composite materials. Addition of tFG to Portland cement results in a significant increase in the compressive strength of the composite, which could potentially reduce energy use and greenhouse gas emissions associated with the cement production. Finally, the cost in energy of producing tFG with the FJH method is <$100 in electricity per ton of rubber waste, which makes the FJH method attractive for manufacturing tFG on a bulk scale while providing an excellent method to upcycle an otherwise pernicious environmental contaminant. This could further result in more widespread usage of tFG in different applications, resulting in lighter and stronger materials at a lower cost.

Disclosure statement

Rice University owns intellectual property on the flash graphene process which has been licensed to Universal Matter. J.M.T. is a stockholder in Universal Matter. But he is not an officer or director in that company. Conflicts of interest are mitigated through regular disclosures to the Rice University office of Sponsored Programs and Research Compliance. C-Crete Technologies owns intellectual property on the strengthening of graphene–cement/concrete composites.

CRediT authorship contribution statement

Paul A. Advincula: Conceptualization, Investigation, Data curation, Writing – original draft, Writing – review & editing. **Duy Xuan Luong:** Investigation. **Weiyin Chen:** Investigation. **Shivaranjan Raghuraman:** Investigation. **Rouzbeh Shahsavari:** Writing – original draft, Supervision, Writing – review & editing. **James M. Tour:** Conceptualization, Writing – original draft, Supervision, Writing – review & editing, Project administration, Funding acquisition.

Declaration of competing interest

The authors declare the following financial interests/personal relationships which may be considered as potential competing interests:

Universal Matter Inc. has licensed from Rice University the FJH approach to graphene. J.M.T. is a stockholder in Universal Matter, but not an employee, officer or director. Potential conflicts of interest are mitigated through regular disclosures to and compliance with Rice University's Office of Sponsored Programs and Research Compliance. C-Crete Technologies owns intellectual property on the strengthening of graphene–cement/concrete composites.

Acknowledgements

The Air Force Office of Scientific Research (FA9550-19-1-0296) and the DOE-NETL (DE-FE0031794) funded this work.

Appendix A. Supplementary data

Supplementary data to this article can be found online at https://doi.org/10.1016/j.carbon.2021.03.020.

References

[1] USTMA, 2017 U.S. Scrap Tire Management Summary, 2018.
[2] I.M. Khan, S. Kabir, M.A. Alhussain, F.F. Almansoor, Asphalt design using recycled plastic and crumb-rubber waste for sustainable pavement construction, Procedia Eng 145 (2016) 1557–1564.
[3] X. Shu, B. Huang, Recycling of waste tire rubber in asphalt and Portland cement concrete: an overview, Construct. Build. Mater. 67 (PART B) (2014) 217–224.
[4] P.J.M. Monteiro, S.A. Miller, A. Horvath, Towards sustainable concrete, Nat. Mater. 16 (2017) 698–699.
[5] S.A. Miller, A. Horvath, P.J.M. Monteiro, Impacts of booming concrete production on water resources worldwide, Nat. Sustain. 1 (2018) 69–76.
[6] M. Krystek, D. Pakulski, V. Patroniak, M. Górski, L. Szojda, A. Ciesielski, P. Samorì, High-performance graphene-based cementitious composites, Adv. Sci. 6 (2019) 1801195.
[7] K.S. Novoselov, A.K. Geim, S.V. Morozov, D. Jiang, Y. Zhang, S.V. Dubonos, I.V. Grigorieva, A.A. Firsov, Electric field in atomically thin carbon films, Science 306 (2004) 666–669.
[8] S.Y. Toh, K.S. Loh, S.K. Kamarudin, W.R.W. Daud, Graphene production via electrochemical reduction of graphene oxide: synthesis and characterisation, Chem. Eng. J. 251 (2014) 422–434.
[9] J. Chen, B. Yao, C. Li, G. Shi, An improved hummers method for eco-friendly synthesis of graphene oxide, Carbon 64 (2013) 225–229.
[10] Y. Hernandez, V. Nicolosi, M. Lotya, F.M. Blighe, Z. Sun, S. De, I.T. McGovern, B. Holland, M. Byrne, Y.K. Gun'ko, J.J. Boland, P. Niraj, G. Duesberg, S. Krishnamurthy, R. Goodhue, J. Hutchison, V. Scardaci, A.C. Ferrari, J.N. Coleman, High-yield production of graphene by liquid-phase exfoliation of graphite, Nat. Nanotechnol. 3 (2008) 563–568.
[11] W. Kong, H. Kum, S.H. Bae, J. Shim, H. Kim, L. Kong, Y. Meng, K. Wang, C. Kim,

J. Kim, Path towards graphene commercialization from lab to market, Nat. Nanotechnol. 14 (2019) 927–938.
[12] D.X. Luong, K.V. Bets, W.A. Algozeeb, M.G. Stanford, C. Kittrell, W. Chen, R.V. Salvatierra, M. Ren, E.A. McHugh, P.A. Advincula, Z. Wang, M. Bhatt, H. Guo, V. Mancevski, R. Shahsavari, B.I. Yakobson, J.M. Tour, Gram-scale bottom-up flash graphene synthesis, Nature 577 (2020) 647–651.
[13] K.M. Wyss, J.L. Beckham, W. Chen, D.X. Luong, P. Hundi, S. Raghuraman, R. Shahsavari, J.M. Tour, Converting plastic waste pyrolysis ash into flash graphene, Carbon 174 (2021) 430–438.
[14] M.G. Stanford, K.V. Bets, D.X. Luong, P.A. Advincula, W. Chen, J.T. Li, Z. Wang, E.A. McHugh, W.A. Algozeeb, B.I. Yakobson, J.M. Tour, Flash graphene morphologies, ACS Nano 14 (2020) 13691–13699.
[15] P.A. Advincula, A.C. De Leon, B.J. Rodier, J. Kwon, R.C. Advincula, E.B. Pentzer, Accommodating volume change and imparting thermal conductivity by encapsulation of phase change materials in carbon nanoparticles, J. Mater. Chem. A 6 (2018) 2461–2467.
[16] J.A. Garlow, L.K. Barrett, L. Wu, K. Kisslinger, Y. Zhu, J.F. Pulecio, Large-area growth of turbostratic graphene on Ni(111) via physical vapor deposition, Sci. Rep. 6 (2016) 1–11.
[17] R. Rao, R. Podila, R. Tsuchikawa, J. Katoch, D. Tishler, A.M. Rao, M. Ishigami, Effects of layer stacking on the combination Raman modes in graphene, ACS Nano 5 (2011) 1594–1599.
[18] C. Cong, T. Yu, R. Saito, G.F. Dresselhaus, M.S. Dresselhaus, Second-order overtone and combination Raman modes of graphene layers in the range of 1690-2150 Cm^{-1}, ACS Nano 5 (2011) 1600–1605.
[19] A. Niilisk, J. Kozlova, H. Alles, J. Aarik, V. Sammelselg, Raman characterization of stacking in multi-layer graphene grown on Ni, Carbon 98 (2016) 658–665.
[20] Z.Q. Li, C.J. Lu, Z.P. Xia, Y. Zhou, Z. Luo, X-ray diffraction patterns of graphite and turbostratic carbon, Carbon 45 (2007) 1686–1695.